A&A 615, A140 (2018)
https://doi.org/10.1051/0004-6361/201832994

Astronomy & Astrophysics

Rotational spectroscopy of the two conformers of 3-methylbutyronitrile (C_4H_9CN) between 2 and 400 GHz⋆

Nadine Wehres[1], Marius Hermanns[1], Olivia H. Wilkins[1,⋆], Kirill Borisov[1], Frank Lewen[1], Jens-Uwe Grabow[2], Stephan Schlemmer[1], and Holger S. P. Müller[1]

[1] I. Physikalisches Institut, Universität zu Köln, Zülpicher Str. 77, 50937 Köln, Germany
e-mail: wehres@ph1.uni-koeln.de, hspm@ph1.uni-koeln.de
[2] Institut für Physikalische Chemie & Elektrochemie, Gottfried-Wilhelm-Leibniz-Universität Hannover, Callinstr. 3A, 30167 Hannover, Germany

Received 9 March 2018 / Accepted 10 April 2018

ABSTRACT

We present high-resolution rotational spectroscopy of the two conformers of 3-methylbutyronitrile (C_4H_9CN). Spectra were taken between 2 and 24 GHz by means of Fourier transform microwave spectroscopy. Spectra between 36 and 403 GHz were recorded by means of frequency modulated (FM) absorption spectroscopy. The analysis yields precise rotational constants and higher order distortion constants, as well as a set of ^{14}N nuclear electric quadrupole coupling parameters for each of the two conformers. In addition, quantum chemical calculations were performed in order to assist the assignments. Frequency calculations yield insight into the vibrational energy structure of the two conformers, from which partition functions and vibrational correction factors are determined. These factors are used to determine experimentally and computationally the energy difference between the two conformers, which is revealed to be negligible. Overall, this study provides precise spectroscopic constants for the search of 3-methylbutyronitrile in the interstellar medium. In particular, this molecule is a perfect test case for our knowledge of branched molecule formation in space.

Key words. laboratory: molecular – techniques: spectroscopic – radio lines: ISM – ISM: molecules – astrochemistry

1. Introduction

Until now, about 200 molecules have been detected in the interstellar and circumstellar medium (ISM and CSM) mainly by means of their rotational transitions in the radio frequency to submillimetre regime. For an overview of identified molecules, we refer the reader to the Cologne Database for Molecular Spectroscopy (CDMS; Müller et al. 2001, 2005; Endres et al. 2016)[1] or to the astrochymist website[2]. Especially for more complex molecules, laboratory data and the knowledge of precise rotational parameters is mandatory before identification of molecules in observational datasets becomes feasible. The spectroscopic parameters can be used to simulate the spectra at different temperatures, which can lead to the identification of molecules in astronomical spectra. Knowledge of complex molecules, in particular branched molecules, can give more insight into the formation pathways of complex species in space. Most of the amino acids which are the building blocks of proteins and which are commonly found in meteoritic material also show a branched structure (for a more recent overview, see Martins et al. 2015 and Iglesias-Groth et al. 2011). However, to date only a single branched molecule, namely *iso*-propyl cyanide (C_3H_7CN), which will be discussed below, has been detected in star-forming regions. This finding lends weight to the idea that biologically important molecules, like amino acids, were produced even before the process of star and planet formation.

The subject of our present study, 3-methylbutyronitrile (C_4H_9CN), belongs to the family of branched alkyl cyanides. Some alkyl cyanides (mostly straight chain) have been studied extensively in the past. Methyl cyanide (CH_3CN; Bocquet et al. 1988; Tam 1988; Pearson & Mueller 1996; Nguyen et al. 2013; Müller et al. 2015, 2016a) and ethyl cyanide (C_2H_5CN; Mäder et al. 1974; Demyk et al. 2007; Brauer et al. 2009; Margulès et al. 2009, 2016; Fortman et al. 2010b,a; Richard et al. 2012; Daly et al. 2013; Pienkina et al. 2017) are the smallest members of this family. Both molecules are commonly found in interstellar environments, especially in star-forming regions such as Sgr A and Sgr B, and in the Orion Nebula (OMC-1) by means of their millimetre wave transitions (Solomon et al. 1971; Johnson et al. 1977; Mehringer et al. 2004; Demyk et al. 2007; Daly et al. 2013). Because of the very high fractional abundances of the cyanide species in observations, the deuterated and ^{13}C-doubly substituted isotopic species could also be identified (Belloche et al. 2016; Margulès et al. 2016). Furthermore, methyl cyanide and ethyl cyanide were also identified in comets, for example in T7 LINEAR and Q4 NEAT (Remijan et al. 2006, 2008), and in Titan's atmosphere, which is known to be rich in nitrogen and methane (Cordiner et al. 2015).

The next largest member of the alkyl cyanide family, propyl cyanide, exists in two different structural isomers, the *normal* straight-chain molecule and the branched *iso*-propyl cyanide (*i*-C_3H_7CN, also called *iso*-butyronitrile). Both molecules have

⋆ The FITS files obtained from SPFIT for the gauche and anti conformer are available at the CDS via anonymous ftp to cdsarc.u-strasbg.fr (130.79.128.5) or via http://cdsarc.u-strasbg.fr/viz-bin/qcat?J/A+A/615/A140

⋆ Current address: Division of Chemistry and Chemical Engineering, California Institute of Technology, Pasadena, CA 91125, USA.

[1] https://www.astro.uni-koeln.de/cdms/entries

[2] http://www.astrochymist.org/

been identified in Sgr B2(N2) within the unbiased spectral line survey Exploring Molecular Complexity with ALMA (EMoCA; Belloche et al. 2014, 2016) using the Atacama Large Millimeter/submillimeter Array (ALMA). Rotational transitions coming from the ground vibrational state and in addition from four low-lying vibrational states of *n*-propyl cyanide have been identified in the laboratory and in space (Müller et al. 2016b). More recent laboratory investigations include up to ten vibrationally excited states of iso-propyl cyanide (Arenas et al. 2017) and a comprehensive study on *iso*-propyl cyanide up to 480 GHz (Kolesniková et al. 2017). To date *iso*-propyl cyanide remains the only branched molecule that has been identified in the interstellar medium. This branched molecule forms the basis for the discussion that other biologically relevant molecules, i.e. amino acids, may form in space.

The next most complex alkyl cyanides are the butyl cyanides (C_4H_9CN). They exist in four different isomers: the straight-chain *normal*-butyl cyanide, the branched 2-cyanobutane (2-methylbutyronitrile) and 3-methylbutyronitrile (*iso*-butyl cyanide), and the doubly branched *tertiary* butyl cyanide (*t*- or *tert*-butyl cyanide). Figure 1 shows the lowest energy conformers for each of the four isomers. In particular, the conformers of 3-methylbutyronitrile are obtained by rotating the methyl or cyanide group around the central carbon–carbon bond (2nd and 3rd carbon atom counted from the cyanide group) as shown in Fig. 2. The two different conformers that result from the rotation in 3-methylbutyronitrile are called the *anti*-conformer (on the left and middle) and the *gauche*-conformer (on the right).

None of the molecules depicted in Fig. 1 have yet been identified in space. Laboratory spectra of three of the five straight-chain *n*-butyl cyanide conformers have already been analysed, and precise spectroscopic parameters were obtained (Bohn et al. 1997; Ordu et al. 2012). A search for this molecule in the EMoCA-survey did not yield any detection. However, more recent astrochemical calculations predict the abundance of this molecule to be just short of the detection limit of the EMoCA-survey (Garrod et al. 2017).

Radio and submillimetre spectra of 2-cyanobutane have also recently been obtained by the Cologne Spectroscopy group, and analysis on the first of three conformers has been completed (Müller et al. 2017). For the two molecules, 2-cyanobutane and 3-methylbutyronitrile, infrared and Raman spectra were obtained previously (Crowder 1988; Crowder & Carlisle 1991). In the case of *tertiary*-butyl cyanide, only one conformer exists which has been studied spectroscopically (Kisiel 1985, 1989; Cazzoli et al. 1993; Kisiel et al. 2001).

We recorded rotational spectra of 3-methylbutyronitrile in the gas-phase in the present study. Quantum mechanical calculations assisted the assignment of the spectra, resulting in precise rotational constants and higher order distortion constants, as well as ^{14}N nuclear electric quadrupole coupling constants for both of the two conformers, i.e. 3-methyl-*gauche*-butyronitrile and 3-methyl-*anti*-butyronitrile. This information can be used for the detection and identification of 3-methylbutyronitrile in interstellar environments. This could lead to more insight into the formation and destruction schemes of complex organic branched molecules in space (Garrod et al. 2017). Furthermore, branched molecules in the interstellar medium might provide a link between complex non-branched straight-chain molecules found in circumstellar material and branched molecules found commonly on meteoritic material.

The paper is structured as follows. First we give an overview of the applied experimental and computational methods in Sect. 2. We present the results in Sect. 3, where we present the spectroscopic assignment, and evaluate the vibrational energy structure and the resulting energy differences between the two conformers. This is followed by Sect. 4 where we discuss the results and compare the outcome to other alkyl cyanide species. The paper finishes with our conclusions in Sect. 5, including implications of future observations and an outlook on complex species in astrophysical environments.

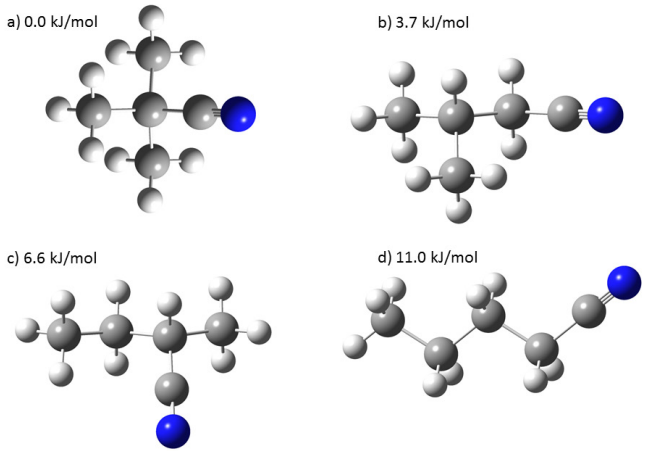

Fig. 1. Structures and relative energies of the four different isomers of butyl cyanide. Here, the lowest energy conformers are shown. *Panel a*: the lowest energy isomer is *tertiary* butyl cyanide (0.0 kJ mol^{-1}). *Panel b*: 3-methylbutyronitrile (here the *anti*-conformer is shown) has an energy difference of 3.7 kJ mol^{-1}. Both conformers, the *anti*- and *gauche*-conformer, are essentially isoenergetic. *Panel c*: 2-cyano-*anti*-butane is about 6.6 kJ mol^{-1} higher in energy. *Panel d*: the highest energy isomer is the straight-chain butyl cyanide (here the *anti–anti*-conformer is shown) with an energy of 11.0 kJ mol^{-1} higher than the lowest energy isomer *tertiary* butyl cyanide. Blue and grey spheres indicate N and C atoms, respectively, and white spheres indicate H atoms.

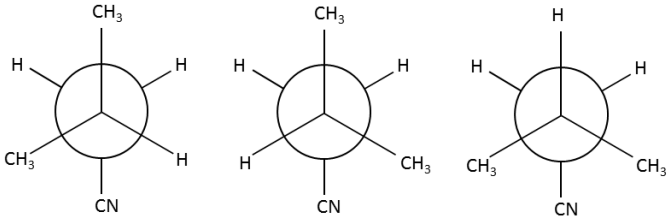

Fig. 2. Newman projections of the two conformers of 3-methylbutyronitrile. *Left and middle panels*: 3-methyl-*anti*-butyronitrile, the two projections are equivalent. *Right panel*: 3-methyl-*gauche*-butyronitrile. The *anti*-conformer thus has twice the statistical weight of the *gauche*-conformer.

2. Methods

2.1. Experimental details

Initial Fourier transform microwave (FTMW) measurements were carried out at the Leibniz Universität Hannover. For this, a small amount of a commercial sample of 3-methylbutyronitrile (TCI Europe N.V.) was highly diluted with neon to a total pressure of 100 kPa. Spectra were taken over a period of several hours with the in-phase/quadrature-phase-modulation passage-acquired-coherence technique (IMPACT) spectrometer to obtain an overview of all lines (Jahn et al. 2012). A single 2 watt chirped selective sideband excitation signal was coupled with a double polarisation rim horn antenna via two parabolic mirrors into a

molecular jet of our sample molecules. The repetition rate was set to 10 Hz. The polarisation of the free induction decay (FID) signal was changed by 90° using a rooftop mirror, incorporating the jet nozzle. Detection was accomplished by using the opposite port of the antenna employing an IQ (in-phase/ quadrature) heterodyne mixer. Upper and lower sidebands were separated by roughly 15 dB in intensity. Spectra with bandwidth of 1 GHz were taken with centre frequencies of 14.9, 15.9, and 22.7 GHz. Subsequently, spectra of 3-methylbutyronitrile were recorded between 2.8 and 24 GHz using a supersonic-jet FTMW spectrometer in the coaxially oriented beam-resonator arrangement (COBRA) using a widely tunable (2 – 26.5 GHz) and very sensitive set-up (Balle & Flygare 1981; Grabow & Stahl 1990; Grabow et al. 2005). Each molecular signal was split by the Doppler effect as a result of the coaxial propagation of the supersonic jet along the resonator axis in the COBRA set-up. Rest frequencies were calculated as the arithmetic mean of the two Doppler components and are in general accurate to about 1 kHz.

Millimetre and submillimetre spectra covering the frequency range between 36 and 403 GHz were recorded at the Cologne Center for Terahertz Spectroscopy at the Universität zu Köln using the MIDAS-COINS and the Cologne (Sub)Millimeter Wave Spectrometer (Ordu et al. 2012; Martin-Drumel et al. 2015), respectively. For these experiments we used a commercial sample of 3-methylbutyronitrile (also TCI Europe N.V.) with a minimum purity of 98%.

The first and second frequency ranges were covered by the MIDAS-COINS spectrometer between 36 and 66 GHz, and between 90 and 126 GHz (Ordu et al. 2012). In summary, for frequencies between 36 and 66 GHz, the frequency output of an Agilent E8257D microwave synthesizer, referenced to a 10 MHz Rubidium clock, was directly guided through a focussing lens into two 7 m long double pass glass-cells with diameters of 10 cm. A Rohde & Schwarz SMF 100A synthesizer was coupled into a frequency amplifier and multiplier chain (VDI, x3) for frequencies between 90 and 126 GHz. A rooftop mirror was used to reflect the beam and to rotate the polarisation by 90°. A wiregrid separated the source beam from the detector beam. A Schottky-type detector from Virginia Diodes was used to record the spectra. The synthesizer was frequency modulated for improved sensitivity, and phase sensitive detection was accomplished using a lock-in amplifier (EG&G Instruments) at twice the modulation frequency resulting in approximately second derivative lineshapes. Fine tuning of the modulation depths versus line strengths resulted in optimum S/N at pressures around 1 Pa. Typical integration times were of the order of 100 ms per data point. Steps between adjacent frequency points are of the order of 30 kHz. The sample flask had to be heated to ambient temperatures (≈50°C) to allow for sufficient vapour pressure throughout the experiment.

The third and fourth frequency ranges were recorded between 175 and 202 GHz and between 360 and 405 GHz, respectively. Details of the spectrometer are mentioned elsewhere (Martin-Drumel et al. 2015). In short, frequency multipliers, driven by a Rohde & Schwarz SMF 100A synthesizer referenced to a 10 MHz Rubidium clock, and Schottky diode detectors were used to record the spectra. Integration times were of the order of 20 ms per data point. The step size between adjacent data points was increased from 54 to 108 kHz between 200 and 400 GHz, respectively.

Overall, the S/N changed with frequency. Although amplifier-multiplier chains usually give less power output with higher frequency, this is balanced by an increase in population density at higher frequencies and by an increase in the Einstein coefficients. Hence, the S/N increased by a factor of 300 between 50 and 400 GHz for strong lines in the spectrum. Although no absolute intensity calibration was performed, relative intensities for close-lying frequency ranges are usually good enough and are frequently used to discriminate between predicted and experimentally obtained lines. Uncertainties were estimated to be roughly half the step size for most of the transitions.

2.2. Quantum chemical calculations

The Gaussian 09 suite of programs (Frisch et al. 2016) was used at the Regionales Rechenzentrum der Universität zu Köln (RRZK) to optimise the geometries, dipole moments, and rotational constants for the *anti*- and *gauche*-conformers of 3-methylbutyronitrile. Frequency calculations to obtain quartic distortion constants as well as starting parameters for the ^{14}N nuclear quadrupole coupling parameters were also obtained. Initially, we applied the B3LYP method (Lee et al. 1988; Becke 1993), followed by the MP2 and MP3 methods (Møller & Plesset 1934). We also carried out MP3/aug-cc-pVTZ calculations at the MP2/aug-cc-pVTZ optimised geometries (MP3(MP2)). These methods were used with the correlation consistent basis-sets cc-pVTZ with diffuse basis functions, augmented cc-pVTZ (Dunning 1989). An overview of the results including applied methods and basis sets is given in Table 1. The table is divided into two sections; the upper part gives the results for the *anti*-conformer and the lower part summarises the results for the *gauche*-conformer. All parameters are directly compared to the experimentally obtained values mentioned in the first column.

2.3. Properties of 3-methylbutyronitrile

3-Methylbutyronitrile comes in two different conformers which are shown in Fig. 2 as Newman projections. The representations on the left-hand side and in the middle show 3-methyl-*anti*-butyronitrile; the cyanide (CN or nitrile) group is located in *anti*-position with respect to one of the methyl (CH_3) groups. On the right-hand side, the Newman projection of 3-methyl-*gauche*-butyronitrile is shown; both methyl groups are in *gauche* position with respect to the cyanide group. It can also be seen that the *anti*-conformer has twice the statistical weight of the *gauche*-conformer, as both projections (on the left and in the middle) are equivalent. This has direct influence on the line strengths in the experimental spectra, such that the intensities of the *anti*-conformer are in general twice as strong as those of the *gauche*-conformer.

Using the rotational constants shown in Table 2, we calculated Ray's asymmetry parameter for both conformers with $\kappa = -0.877$. The deviation from the experimentally found κ is quite low (≤1%) for both conformers, indicating that this molecule is an asymmetric rotor moderately close to the prolate limit of −1. Successive *R*-type transitions will thus show a spacing of roughly $B + C \approx 4.6$ GHz for the *gauche* and 3.8 GHz for the *anti*-conformer.

Both rotamers can be obtained when rotating the third carbon atom (the first carbon atom is counted from the cyanide group) by 120°. This also leads to two different symmetry groups of the conformers. The C_1-symmetry for the *anti*-conformer shows a zig-zag configuration with four carbon atoms located coplanar spanning a dihedral angle of about 174°, while the C_s-symmetry for the *gauche*-conformer has three carbon atoms coplanar and the two methyl groups projected out of the plane. The resulting symmetry groups, i.e. the C_1 and C_s symmetry, have influence on the energy level structure of the molecule, which is described in more detail in Sect. 3.3.

Table 1. Experimental results and quantum chemical calculations for the two conformers of 3-methylbutyronitrile.

Parameter	Exp.	B3LYP/cc-PVTZ	MP2/cc-pVTZ	MP2/aug-cc-pVTZ	MP3/cc-pVTZ	MP3(MP2)/aug-cc-pVTZ[a]
			anti-conformer[b]			
ΔE		0	0.9	0.9	0	0
A	7363.75	7348.75	7446.01	7443.70	7410.54	
B	2107.16	2089.74	2121.59	2124.01	2110.98	
C	1762.08	1749.23	1776.53	1777.91	1767.50	
$D_K \times 10^3$	2.470	2.552585	2.767820			
$D_{JK} \times 10^3$	4.022	4.258574	4.122134			
$D_J \times 10^3$	0.346	0.326543	0.360434			
$d_1 \times 10^6$	−68.780	−64.893	−71.733			
$d_2 \times 10^6$	−20.464	−20.582	−20.757			
χ_{aa}	−3.077	−3.500	−2.867	−2.822	−3.370	−3.149
χ_{bb}	1.248	1.456	1.155	1.131	1.378	1.259
χ_{cc}	1.829[c]	2.044	1.712	1.691	1.991	1.891
χ_z		−4.731	−3.933			−4.311
η		0.035	0.022			0.027
μ_a		3.901	3.741	3.860	3.823	3.943
μ_b		1.112	1.102	1.136	1.121	1.168
μ_c		0.561	0.516	0.526	0.547	0.543
κ	−0.8768	−0.8784	−0.8783	−0.8778	−0.8783	
			gauche-conformer[d]			
ΔE		0.9	0	0	0.1	0.2
A	5293.82	5351.55	5308.52	5301.35	5332.73	
B	2456.44	2411.15	2485.240	2489.13	2458.71	
C	2270.25	2217.70	2306.780	2310.97	2272.44	
$D_K \times 10^3$	−2.780	−3.966136	−2.858301			
$D_{JK} \times 10^3$	4.610	5.842707	4.550832			
$D_J \times 10^3$	1.109	1.037313	1.165022			
$d_1 \times 10^6$	36.301	22.157	44.040			
$d_2 \times 10^6$	4.096	-4.750	5.569			
χ_{aa}	−1.440	−1.723	−1.330	−1.297	−1.604	−1.4531
χ_{bb}	2.011	2.264	1.904	1.874	2.207	2.074
χ_{cc}	−0.571[c]	−0.541	−0.574	−0.576	−0.603	−0.621
χ_{ac}	3.1	3.555	2.963	2.921	3.445	3.246
χ_z		−4.706	−4.735			−4.310
η		0.0439	0.033			0.037
μ_a		3.364	3.188	3.289	3.277	3.362
μ_b		0.000	0.000	0.000	0.000	0.000
μ_c		2.240	2.183	2.252	2.238	2.311
κ	−0.8768	−0.8765	-0.8811	−0.8808	−0.8783	

Notes. Relative energies (ΔE in kJ mol^{-1}), as well as rotational constants (MHz), ^{14}N nuclear electric quadrupole coupling parameters (MHz), and dipole moment components (Debye) are given. The dimensionless asymmetry parameter η^e and Ray's asymmetry parameter κ^f (dimensionless) were determined. [a]Geometries are based on MP2 calculations; [b]C_1-symmetry; [c]derived values; [d]C_s-symmetry; [e]$\eta = (\chi_x - \chi_y)/\chi_z$; [f]$\kappa = (2B - A - C)/(A - C)$.

The dipole moment component along the *a*-axis is roughly 3.2 D and 3.8 D for the *gauche*- and *anti*-conformers, respectively, and mainly caused by the cyanide group (CN group). Additionally, the dipole moment component along the *b*-axis of the *gauche*-conformer is absent, leading to only *a*- and *c*-type transitions for the *gauche*-conformer.

3. Results

3.1. Spectral assignment of 3-methyl-*gauche*-butyronitrile

Figure 3 shows part of the recorded FTMW spectrum around 19 GHz obtained with the COBRA spectrometer. A pattern of 3-methyl-*gauche*-butyronitrile *a*-type transitions is identified as predicted from initial B3LYP and MP2 calculations. Here, strong *a*-type transitions consisting of $K_c = J$, $J = 4$–3, and $K_a = 0$ are identified. Due to the experimental set-up the lines are split into two Doppler components. This is caused by having the jet-expansion parallel to the microwave emission. The rest frequencies are indicated in the figure, as are the two Doppler components for each transition. Each rotational level with $J \geq 1$ is split into three hyperfine components caused by the electric quadrupole moment of the ^{14}N nucleus ($I = 1$). The final quantum number F therefore takes values of J and $J \pm 1$, where the upper and lower state F quantum numbers are allowed to differ by 0 and ±1. The hyperfine splitting is usually larger at lower

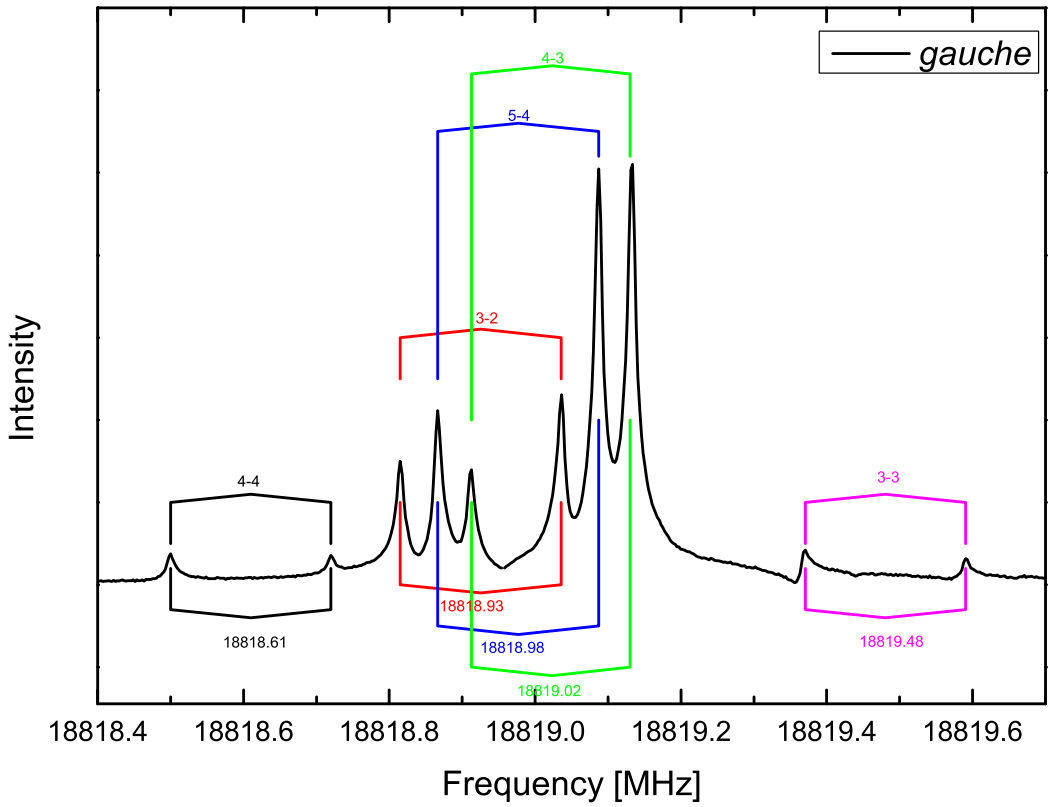

Fig. 3. FTMW spectrum of the *gauche*-conformer of 3-methylbutyronitrile. The spectral lines in the jet-experiment are split into two Doppler components since the microwave emission is parallel to the supersonic jet expansion. The actual frequency is indicated in the figure and is determined by calculating the arithmetic mean of the two Doppler components. The hyperfine splitting due to the ^{14}N nucleus is obvious. Here, the transition $J_{Ka,Kc} = 4_{0,4}–3_{0,3}$ is split into five components. The F quantum numbers are shown above each transition.

J values and thus at lower frequencies. Five out of six hyperfine transitions can thus be distinguished in Fig. 3 and can help to secure the assignments. The hyperfine splitting with the respective F quantum numbers are given as superscripts in the figure. Assignments were extended by using Pickett's SPFIT/SPCAT suite of programs (Pickett 1991).

After the first assignments were made, new predictions using better rotational constants were obtained. A total of about 100 transitions were assigned between 2.8 and 24.0 GHz using the FTMW spectra. The transitions included J quantum numbers between 1 and 8 as well as K_a up to 4. We assigned a-type and c-type transitions for mainly R-type and only some Q-type transitions. The most frequently assigned transitions are a-type transitions. Overall, the FTMW data were reproduced well using quartic centrifugal distortion constants as well as the diagonal ^{14}N nuclear electric quadrupole coupling parameters χ_{aa} and χ_{bb}. The off-diagonal component, χ_{ac}, was estimated and kept fixed during the fit, because the parameter affected some transitions, but was only barely determined (χ_{ac} = 2.76 ± 0.90 MHz).

These assignments allowed us to obtain better predictions for the higher frequency ranges, i.e. between 40 and 70 GHz, and between 90 and 125.6 GHz. We were able to assign almost 900 transitions in these spectral regimes with J quantum numbers up to J = 80 and up to K_a = 24. The assigned transitions were Q- and R-type transitions; about 50% of the lines are Q-type transitions, and 50% R-type transitions. Again, a-type and c-type transitions were assigned; about 330 transitions were assigned a-type transitions, and almost 560 c-type transitions.

The frequency ranges between 175 and 206.2 GHz and between 360 and 403 GHz were analysed subsequently. Here, about 1600 lines were assigned. Out of these lines about 1530 transitions were assigned R-type transitions, the rest Q-type transitions. The K_a quantum number reaches values of up to 61. Most of these transitions are a-type transitions (more than 1100) and about 480 c-type transitions.

The final set of spectroscopic parameters is summarised in Table 2. The experimental lines were fitted using experimental uncertainties. An RMS error of 0.89 was obtained for a fit that includes about 2600 transitions and 20 parameters. Overall, the experimental spectrum was quite well reproduced using quartic, sextic, and some octic centrifugal distortion constants, as well as the ^{14}N nuclear electric quadrupole coupling parameters χ_{aa}, χ_{bb}, and χ_{ac}.

3.2. Spectral assignment of 3-methyl-*anti*-butyronitrile

Figure 4 shows part of the FTMW spectrum around 16 GHz of 3-methylbutyronitrile, *anti*-conformer. All peaks show two Doppler components because of the experimental set-up where the axis of the jet-expansion is parallel to the microwave propagation. The two Doppler components which belong together are marked, and the resulting rest frequency is simply the arithmetic average of the two respective Doppler components. The rest frequencies are also given in Fig. 4. Here a quintet of lines is shown which belong to the $K_c = J$ with $J = 3–2$ transition, and $K_a = 1–0$ (b-type transitions) as predicted from initial B3LYP and MP2 calculations. Five of the six hyperfine components are clearly visible and the F quantum numbers of the respective transitions are given as superscript.

Table 2. Spectroscopic parameters of the two conformers of 3-methylbutyronitrile (MHz).

Parameter	Value	Value
	gauche-Conformer	*anti*-Conformer
A	5293.815739 (54)	7363.745484 (92)
B	2456.4351918 (226)	2107.1641996 (219)
C	2270.2489771 (220)	1762.0787378 (211)
$D_K \times 10^3$	−2.779842 (154)	2.46956 (165)
$D_{JK} \times 10^3$	4.610103 (59)	4.022356 (122)
$D_J \times 10^3$	1.1092278 (77)	0.3460625 (91)
$d_1 \times 10^6$	36.3007 (56)	−68.7804 (58)
$d_2 \times 10^6$	4.0964 (41)	−20.4636 (50)
$H_K \times 10^9$	−89.044 (95)	−336.55 (244)
$H_{KJ} \times 10^9$	114.864 (52)	−68.055 (102)
$H_{JK} \times 10^9$	−17.0027 (178)	−2.6332 (236)
$H_J \times 10^9$	0.87726 (76)	0.19526 (148)
$h_1 \times 10^9$	−0.15617 (57)	0.05780 (41)
$h_2 \times 10^{12}$	−9.86 (49)	17.74 (36)
$h_3 \times 10^{12}$	2.986 (198)	8.318 (107)
$L_{KKJ} \times 10^{12}$	−0.9083 (180)	−3.1834 (258)
$L_{JK} \times 10^{12}$	−0.1446 (78)	−0.2924 (62)
$L_{JJK} \times 10^{12}$	0.05210 (170)	0.01622 (143)
$L_J \times 10^{15}$		−0.331 (76)
$l_4 \times 10^{15}$		−0.0295 (53)
χ_{aa}	−1.44002 (59)	−3.07713 (67)
χ_{bb}	2.01104 (76)	1.24843 (87)
χ^a_{cc}	−0.57102 (66)	1.82870 (66)
χ^b_{ac}	3.1	
RMS	0.89	0.92

Notes. Numbers in parentheses are one standard deviation in units of the last significant figure. Watson's S reduction in the I^r representation was used. [(a)]Derived values. [(b)]Estimated and kept fixed in the fits.

Overall, we assigned more than 110 transitions in the FTMW frequency range, i.e. between 3.8 GHz and 24.2 GHz. The data were reproduced well using quartic centrifugal distortion constants as well as the ^{14}N nuclear electric quadrupole coupling parameters χ_{aa} and χ_{bb}. Almost all of the transitions were *R*-type transitions and only a handful of lines are *Q*-type transitions. About 80 transitions were *a*-type transitions. Additionally, we assigned 26 *b*-type and 5 *c*-type transitions.

The FTMW assignments were then used to obtain more precise predictions for the 3-methylbutyronitrile *anti*-conformer at higher frequencies, i.e. between 38 and 70 GHz and between 90 and 127 GHz. Here, a total of more than 750 lines were added to the assignments. Of these lines, we assigned 14 *Q*-type transitions, the rest are *R*-type transitions. About 30 *b*-type transitions were assigned, the rest are assigned *a*-type transitions. No *c*-type transitions could be assigned. The K_a quantum numbers reached values of up to 29, and J quantum numbers now reach values of up to 37.

In the third and fourth spectral ranges, between 175 and 207 GHz and between 360 and 402 GHz, we assigned about 1500 transitions of which the majority are *a*-type transitions. Only about 40 *b*-type and two *c*-type transitions were assigned. Mainly *R*-type transitions and only about 20 *Q*-type transitions were assigned. J quantum numbers were assigned up to $J = 114$, and K_a quantum numbers reached values of up to $K_a = 60$.

The final set of spectroscopic parameters is summarised in Table 2. The experimental lines were fitted within experimental uncertainties. An RMS error of 0.92 was obtained. In total about 2350 transitions using 22 parameters were fitted, including the rotational constants, quartic, sextic, and even octic distortion constants, as well as the electric quadrupole coupling parameters.

The predictions of rotational spectra for both conformers will be made available in the catalogue section of the ascii version[3] of the CDMS (Müller et al. 2001, 2005). Furthermore, the .fits output files will also be made available in the Virtual Atomic and Molecular Data Centre (VAMDC; Endres et al. 2016) and through the Strasbourg Astronomical Data Center (CDS).

3.3. Vibrational energy structure

3-Methylbutyronitrile shows a very complex spectrum at room-temperature of which only a fraction of lines was assigned. We thus investigated the vibrational energy structure of both conformers in more detail by means of frequency calculations using the Gaussian suite of programs (Frisch et al. 2016). Here, we used the results of the MP2/cc-pVTZ computations. In general, the vibrational energy levels for such a complex molecule (15 atoms) will have significant population at room-temperature in several low-lying energy levels, and thus will contribute significantly to the complexity of the spectrum. Furthermore, this information can be used for further studies focussing on the assignments of vibrationally excited states in the laboratory, and also in the interstellar medium.

Overall, 3-methylbutyronitrile has 39 fundamental vibrations. The lowest vibrational levels are around 86 and 90 cm^{-1} for the *anti*- and *gauche*-conformer, respectively. The *anti*-conformer has C_1 symmetry, thus all vibrations belong to the symmetry class A. However, the *gauche*-conformer has C_s symmetry and hence 22 vibrations belong to the symmetry class A′, and 17 vibrations belong to the symmetry class A″. Within this vibrational manifold, 8 fundamental vibrations are quite low-lying, i.e. below the energy of 500 cm^{-1} for each of the two conformers. This indicates that a fraction of the population can still be found in higher vibrational levels, i.e. at room-temperature about 10% of the population or more relative to the ground state. Including higher harmonics, 6 additional vibrational bands with less than 480 cm^{-1} in energy exist for each of the two conformers. An energy diagram summarising the vibrational manifold is shown in Fig. 5. The energies are given in reciprocal centimetres for the fundamental bands of each conformer. In the middle of the diagram the overtones are indicated by dotted lines. This manifold of vibrational states indicates once more the complexity of the spectrum.

Rotational partition function values ($Q_{\rm rot}$) at seven CDMS standard temperatures plus two additional temperatures (120 and 180 K) are shown in Table 3. The values were determined using the following formula:

$$Q_{\rm rot} = [(kT/h)^3(\pi/ABC)]^{1/2}, \quad (1)$$

where A, B, and C are the rotational constants.

Additionally, we also evaluate contributions of vibrational states to the rotational partition function. For this we calculate vibrational correction factors $F_{\rm vib}$ to the rotational partition

[3] https://www.astro.uni-koeln.de/cdms/entries

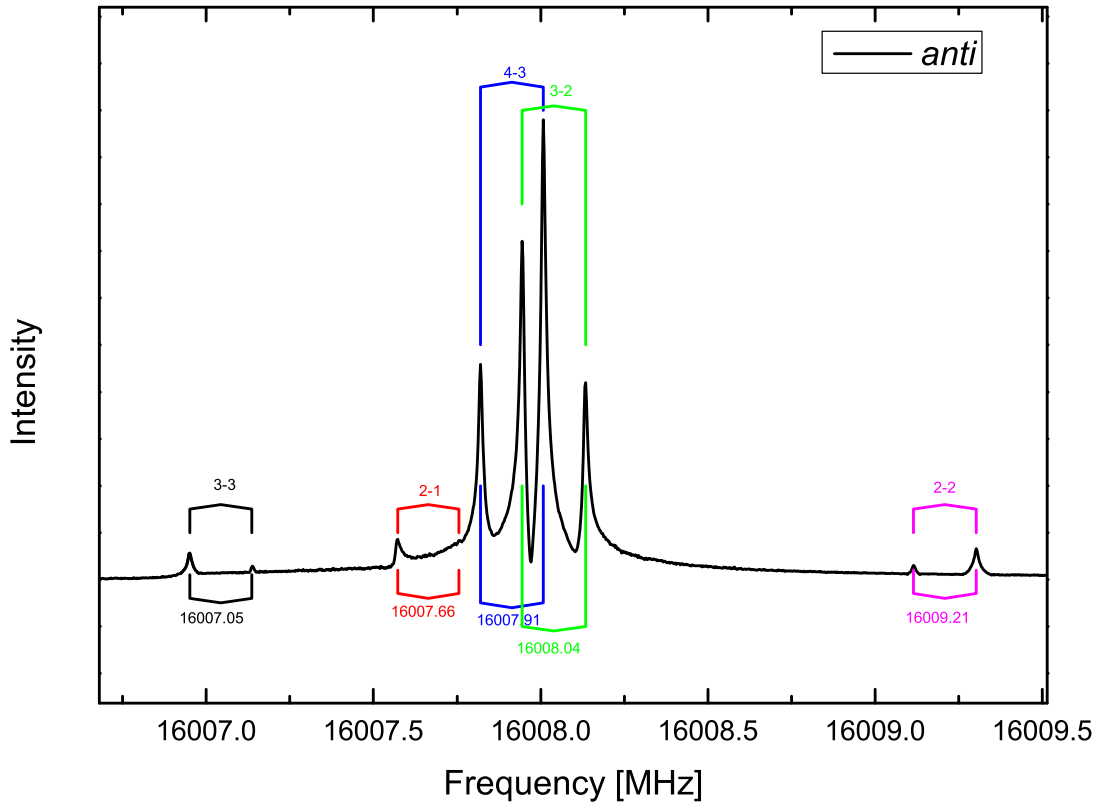

Fig. 4. FTMW spectrum of the *anti*-conformer of 3-methylbutyronitrile is shown. The spectral lines are split in the jet-experiment into two Doppler components since the microwave emission is parallel to the supersonic jet expansion. The actual frequency is indicated and is determined by calculating the arithmetic mean of the two Doppler components. The hyperfine splitting due to the ^{14}N nucleus is obvious. Here, the transition $J_{Ka,Kc} = 3_{1,3}–2_{0,2}$ is split into its five components. The superscript gives the F quantum numbers of the respective transition.

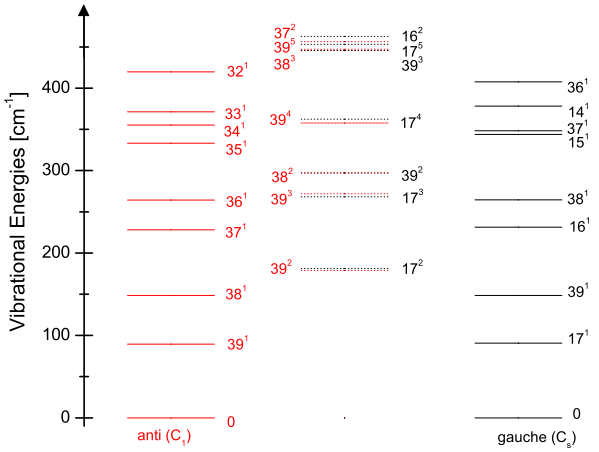

Fig. 5. Energy level diagram of 3-methylbutyronitrile up to 480 cm^{-1}. The *anti*-conformer is shown in red (left); the *gauche*-conformer is shown in black (right). The dotted lines in the centre indicate overtone transitions.

function at the same temperatures using

$$F_{\mathrm{vib}} = \prod_{i=1}^{3N-6} \frac{1}{1 - e^{(-E_i/kT)}}, \qquad (2)$$

where N is the number of atoms in the molecule; thus, the product is formed over the different energies (E_i) including 39 vibrational states. The results are given in Table 3. The vibrational correction factors will be used in the next paragraph to determine experimentally the energy differences of the two conformers more precisely.

3.4. Minimum energies of the two conformers

Comparing the geometry optimised minimum energies obtained from the different quantum chemical calculations in Table 1, it can be seen that both conformers are essentially isoenergetic. Specifically, higher level computations, i.e. MP3/cc-pVTZ and MP3(MP2)/aug-cc-pVTZ, show that the determined energy difference between the *anti*- and *gauche*-conformers is almost negligible, where the latter calculation is based on geometries obtained at the MP2 level. These predictions can be tested via analysis of the experimental spectrum. If both conformers indeed have the same minimum energy, then the *anti*-conformer should be twice as strong in the experimental spectrum for compareable transitions; the factor of two is due to the statistical weight. In general, intensities in frequency modulation (FM) absorption experiments are only approximate, and depend strongly on the variation of source power with frequency. Nonetheless, it can be shown that the intensities can usually be trusted if lines are close together, and that the power of a microwave spectrometer only varies locally, i.e. ≤1 GHz, by a small percent (Medvedev & De Lucia 2007).

In this paragraph we compare the predicted transition intensities to the experimentally found intensities. A plot showing transitions of the *gauche*- and *anti*-conformer is presented as an example in Fig. 6. Here we only take transitions into account that are very close in frequency. The experimentally determined intensity ratios are of the order of 0.65 (*gauche* versus *anti*). The predicted intensity ratios are of the order of 0.78, giving rise

Table 3. Rotational partition function values Q_{rot} and vibrational correction factors F_{vib} to the rotational partition function of 3-methyl-*anti*-butyronitrile and 3-methyl-*gauche*-butyronitrile at selected temperatures.

Temperature [K]	Q_{rot}	F_{vib}
	anti-Conformer	
300.0	167528.1804	29.8662
225.0	108812.7451	9.4436
180.0	77860.0623	4.8536
150.0	59230.1562	3.1820
120.0	42381.6498	2.1516
75.0	20941.0226	1.3242
37.5	7403.76952	1.0371
18.75	2617.6278	1.0012
9.375	925.4712	1.0000
	gauche-Conformer	
300.0	161221.7655	28.6185
225.0	104716.6084	9.1633
180.0	74929.1055	4.7484
150.0	57000.5018	3.1295
120.0	40786.2390	2.1261
75.0	20152.7207	1.3163
37.5	7125.0627	1.0356
18.75	2519.0901	1.0010
9.375	890.6328	1.0000

to an overall intensity ratio of experimental intensities versus predicted intensities of 0.83. The vibrational correction factors calculated above (see also Table 3), as well as the statistical weights of the *anti*- and *gauche*-conformers (2:1, see also Fig. 2) have been taken into account in this analysis. This procedure was performed for several transitions in the frequency range between 179 and 375 GHz, and for a total of 24 transitions resulting in 16 pairs of lines. Overall, we find quite reasonable agreement between predicted line intensities and experimentally found transition intensities. The ratio between predicted and experimentally found intensities varies around 1, with the average being around 1.03 and a 1σ error of 12%. A summary of all transitions that have been taken into account is shown in Table 4. This can be directly translated into an energy difference of +75 J mol^{-1} for the *anti*-conformer, but with an error of ~300 J mol^{-1}.

4. Discussion

The large sets of experimentally determined parameters for both conformers of 3-methylbutyronitrile are summarised in Table 2. The experimental values agree well with the predicted calculations which are shown in Table 1. To obtain the experimental values we used Watson's *S* reduction in the I^r representation. Overall, the rotational constants are quite close for most methods and basis sets and vary by a few MHz up to 90 MHz at most for the *A*-rotational constant. This results in a 1–2% deviation from the experimental results.

The calculations of the dipole moments for both conformers agree within a small percent and should be close to the experimental values, as previous studies indicate for *iso*-propyl cyanide, *anti*-*n*-propyl cyanide, and *cyclo*-propyl cyanide (Müller et al. 2011). For our study the dipole moment components resulting from the B3LYP calculations are used. These results agree closely with the MP3(MP2) calculations, usually within about a 1% deviation from the *A* rotational constant and about 5% for the *B* and *C* rotational constants.

There is a larger scatter in the calculated ^{14}N nuclear electric quadrupole coupling parameters $\chi_{aa}, \chi_{bb}, \chi_{cc}$ as well as the off-diagonal element χ_{ac} of more than 10%. This does not seem to be that uncommon as similar deviations have also been observed for very recent studies on 2-cyanobutane (Müller et al. 2017) and *iso*-propyl cyanide (Müller et al. 2011). Very interestingly, the calculated values using the MP3 method based on the optimised MP2 geometries (MP3(MP2)/aug-cc-pVTZ) are very close to the experimental values, in contrast to the other methods. As mentioned in the study on 2-cyanobutane this seems to be due to cancellation of errors and has also been shown for calculations on methyl cyanide (Müller et al. 2017). Also for this molecule, the best agreement on χ_{ij} is obtained using MP3 values at the geometry of MP2 level calculations. For 3-methylbutyronitrile, the calculated χ_{aa} and χ_{bb} values using the MP3 method (with MP2 geometries) gives deviations of the order of 1% for the diagonal ^{14}N nuclear electric quadrupole coupling constants, whereas the other methods deviate by about 10% from the experimental values. Given that χ_{aa} and χ_{bb} agree very well with the experimental value, we used them to also derive the principal nuclear quadrupole coupling parameter χ_z as well as the principal asymmetry parameter $\eta = (\chi_{xx} - \chi_{yy})/\chi_{zz})$. Thus, χ_z is of the order of −4.311 and −4.310 MHz for the *anti*- and *gauche*-conformers, respectively, still using the MP3 calculations based on MP2 optimised geometries. This is nearly identical to values found for 2-cyanobutane (χ_z = −4.316 MHz) and methyl cyanide (χ_z = −4.314 MHz). Comparable values are also found for *iso*-propyl cyanide, *anti*-*n*-propyl cyanide, and *cyclo*-propyl cyanide (Müller et al. 2011). The asymmetry parameter η of the principal quadrupole tensor seems to be sufficiently close to zero for many alkyl cyanides (Müller et al. 2011). In this respect our calculated values of $\eta = 0.03$ and $\eta = 0.04$ for the *anti*- and *gauche*-conformers seem to agree reasonably well. The only value that differs in this respect is from *cyclo*-propyl cyanide with $\eta = 0.17$, which is quite a bit different from zero and hence the (quadrupole) tensor appears to be less symmetric. This deviation is probably due to coupling between the cyanide group and the ring.

The quantum chemical calculations shown in Table 1 furthermore indicate that the energy difference of the two conformers is almost negligible with 100–200 J mol^{-1} at the MP3/cc-pVTZ and MP3(MP2)/aug-cc-pVTZ level. These results are close to those determined in our experiment, and once more indicate that this level of computation is likely needed to obtain meaningful quantities on such a complex molecule. In this respect the *gauche*-conformer is at slightly higher energies based on the computations. Depending on the level of calculation one or the other conformer is predicted to be lower/higher in energy. The experimental findings give a 3% deviation from parity with about 12% error, and thus imply that the two conformers are essentially isoenergetic. However, a 3% deviation would result in an energy difference of roughly 75 J mol^{-1} (6 cm^{-1} or 9 K) for the *anti*-conformer, but with an error of ≃300 J mol^{-1}. The experimentally determined energy differences have been corrected for the different statistical weights and additionally using the vibrational correction factors. The dipole moments used in this study are based on the results of the B3LYP calculations for both conformers. The determined energy differences can also be compared to a study by Crowder (1988) who, based on molecular mechanics calculations, also concluded that the conformers are very similar in energy. In his study the *anti*-conformer is

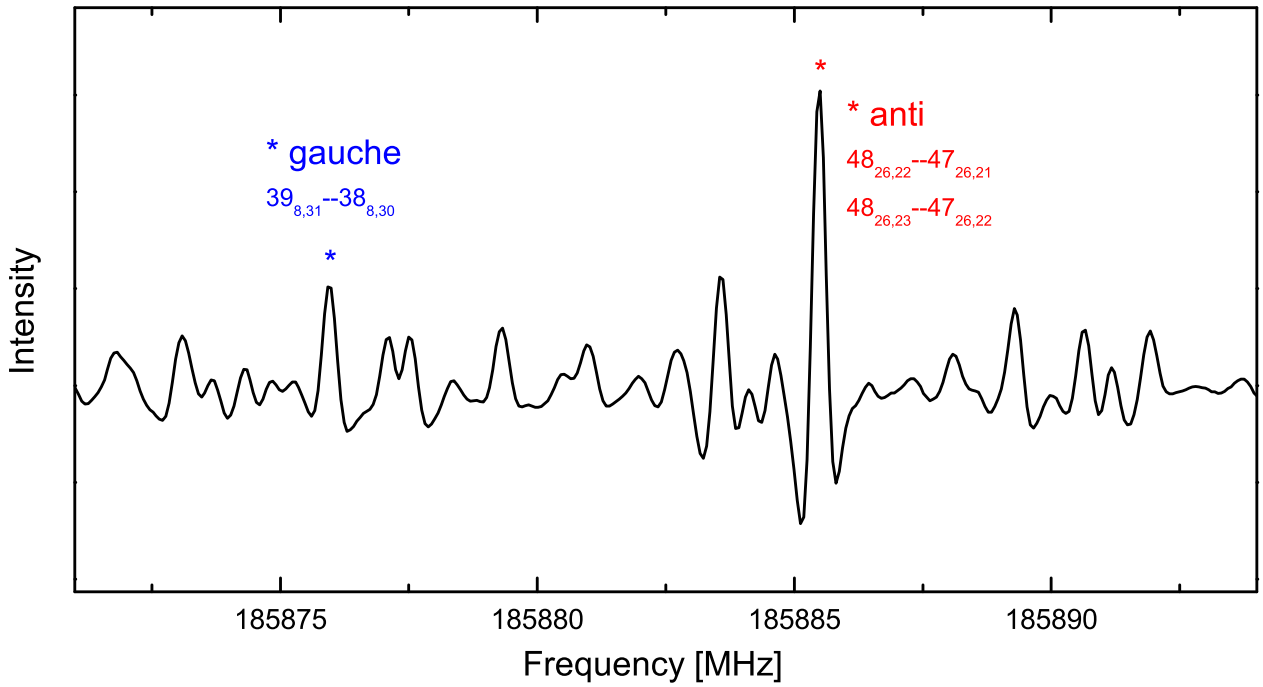

Fig. 6. Excerpt of the 3-methylbutyronitrile spectrum. In red: transitions of 3-methyl-*anti*-butyronitrile. In blue: transitions of 3-methyl-*gauche*-butyronitrile. Among others, these transitions are used to determine the energy difference between the two conformers of 3-methylbutyronitrile (see also Table 4). The results show that the energy difference is negligible.

Table 4. Comparison of relative intensities between predicted and measured lines to determine possible energy differences between the two distinct conformers of 3-methylbutyronitrile.

Conformers	Frequency [MHz]	Experimental ratio	Predicted ratio	$\frac{\text{Experimental ratio}}{\text{Predicted ratio}}$
gauche : *anti*	179780.65 : 179847.28	0.68	0.63	1.09
gauche : *anti*	179780.65 : 179848.36	0.75	0.63	1.19
gauche : *anti*	181864.39 : 181853.98	0.30	0.24	1.25
gauche : *anti*	185875.97 : 185863.15	0.66	0.64	1.04
gauche : *anti*	185875.97 : 185862.21	0.71	0.64	1.11
gauche : *anti*	185875.97 : 185885.47	0.65	0.78	0.83
gauche : *anti*	188169.56 : 188163.25	0.71	0.68	1.04
gauche : *anti*	195666.78 : 195633.48	0.60	0.70	0.85
gauche : *anti*	195656.40 : 195633.48	0.64	0.70	0.91
gauche : *anti*	206144.08 : 206141.00	0.58	0.48	1.21
gauche : *anti*	206144.08 : 206147.46	1.01	0.96	1.06
gauche : *anti*	361509.99 : 361478.16	0.37	0.36	1.01
gauche : *anti*	361509.99 : 361588.62	0.38	0.38	1.00
gauche : *anti*	361509.99 : 361601.38	0.93	0.89	1.04
gauche : *anti*	361509.99 : 361622.40	0.83	0.87	0.95
gauche : *anti*	375080.84 : 375030.46	1.59	1.70	0.93
Average				1.03
Sigma				12%

determined to be slightly lower in energy, i.e. about 100 cal mol^{-1}, which amounts to around 418 J mol^{-1} and thus slightly more than the higher level computations indicate.

Overall, 3-methylbutyronitrile shows a very rich spectrum, originating not only from the two different conformers, but also from many low-lying vibrational levels that are populated at room temperature. The information on the low-lying energy levels can also be of potential interest for astronomers since a study on *n*-propyl cyanide in Sgr B2N showed that the rotational temperatures are of the order of 150 K (Müller et al. 2016b). The lowest lying vibrational level was determined to be around 86 and 90 cm^{-1} for the *anti*- and *gauche*-conformers, respectively (see Sect. 3.3). These values correspond to populations of 0.44 and 0.42, respectively, relative to the ground vibrational states.

The experimental uncertainties in our data around 400 GHz are of the order of 40 kHz at most. With these uncertainties, we predict transitions up to 720 GHz corresponding to the ALMA Band 9 receiver (602–720 GHz). The predictions also include moderately weak and weak transitions, reaching

upper J-quantum numbers of 150. Almost 90% of these transitions fall below a frequency uncertainty of 400 kHz, which we claim to be trustworthy with respect to our experimental frequency uncertainty of 40 kHz and with respect to an expected FWHM of a Doppler broadened line of around 1 MHz at these frequencies (720 GHz). Transitions showing higher uncertainties (≥400 kHz) mainly include lower state energies in excess of 800 cm^{-1} or more than 1100 K. The predictions should thus be accurate enough to identify sufficiently strong transitions in room-temperature laboratory spectra as well as the telescope spectra expected from the ALMA EMoCA-survey.

5. Conclusions and implications

Precise spectroscopic parameters have been obtained for the two conformers of 3-methylbutyronitrile from high-resolution rotational spectroscopy that covers the radio frequency regime up to the submillimetre regime (2–403 GHz). The experimental analysis yielded rotational and higher order distortion constants. Additionally, we could determine two out of three ^{14}N nuclear electric quadrupole coupling parameters for each conformer (χ_{aa} and χ_{bb}) experimentally; χ_{cc} was subsequently derived from χ_{aa} and χ_{bb}. Furthermore, we investigated the vibrational energy levels and conclude that many of the vibrationally excited states show significant population at room temperature and thus contribute to the complexity of the experimental spectrum. These low-lying vibrationally excited states could potentially also play a role in the interstellar medium. Finally, we show that both conformers, i.e. the *anti*- and *gauche*-conformers of 3-methylbutyronitrile, are essentially isoenergetic. This study can thus be used for comparison to observational data in order to identify both conformers of 3-methylbutyronitrile in warm and dense parts of star-forming regions where larger alkyl cyanides are playing an important role.

In general, cyanide species have been identified in space before and are often used as tracers of the physical and chemical conditions in space; methyl cyanide, for example, is frequently used as a temperature tracer. However, the identification of the first branched cyanide species, *iso*-propyl cyanide, enhances discussion on the formation mechanisms of branched molecules in general in the interstellar and circumstellar medium (Garrod et al. 2017). Although a search for *n*-butyl cyanide in the EMoCA-survey yielded no detection (Belloche et al. 2014, 2016), it was argued that the structural (branched) isomers of butyl cyanide, 2-cyanobutane followed by 3-methylbutyronitrile, should show higher abundances under interstellar conditions compared to *n*-butyl cyanide. The abundance of *tertiary* butyl cyanide, however, is predicted to be almost negligible compared to the abundances of the other isomers of the butyl cyanide species (Garrod et al. 2017). In this study the upper limit on the column density of *n*-butyl cyanide is said to be 1.5 times lower than the column density of *n*-propyl cyanide, which then translates into a factor of 1.7 in terms of abundance with respect to H_2. The resulting upper limit on the abundance ratio of *n*-C_4H_9CN/*n*-C_3H_7CN is thus given with 0.59. Since the abundance of *n*-butyl cyanide was found to be just short of the detection limits in the EMoCA-survey, new ALMA cycle 4 observations were requested which may yield sufficiently high S/N for the detection of 3-methylbutyronitrile, as well as 2-cyanobutane.

Following the abundance predictions, it is argued that the kinetics on the formation route is more important than the thermodynamic stability with respect to the abundances in space (Garrod et al. 2017). This conclusion is in line with findings that molecular clouds are generally not in thermodynamic equilibrium and hence also allow for the detection of many unsaturated species, attesting the importance of kinetics over thermodynamics (Tielens 2013). Hence, 3-methylbutyronitrile and 2-cyanobutane are the perfect test candidates to improve our knowledge on the formation pathways of cyanides in the interstellar and circumstellar medium (Garrod et al. 2017). A comparison between the model predictions of Belloche et al. (2014) and Garrod et al. (2017) seem to indicate that the main formation pathway for branched cyanide species is not the addition of CN to propane (C_3H_7), but rather the addition of the methyl group (CH_3) to the secondary radical of ethyl cyanide (C_2H_4CN). With these reaction schemes the abundance ratios for *n*-propyl cyanide and *iso*-propyl cyanide were obtained and matched the observations better. A possible detection of 3-methylbutyronitrile in observational datasets will then put constraints on the formation schemes for complex (branched) organic species in the interstellar and circumstellar medium.

Additionally, these types of molecules (alkyl cyanides) are also likely to be present in the nitrogen-rich atmopshere of Saturn's moon Titan. The methane- and ethane-rich seas interact with the nitrogen atmosphere to form the most common organic nitrogen species observed in Titan's upper atmosphere, such as hydrogen cyanide (HCN), methyl cyanide (CH_3CN), ethyl canide (C_2H_5CN), vinyl cyanide (C_2H_3CN) cyanoacetylene (HC_3N), as well as cyanoallene (C_4H_3N) and 2,4-pentadynenitrile (HC_5N) (Stevenson et al. 2015; Cordiner et al. 2015; Palmer et al. 2017; Lai et al. 2017). In addition, propane has tentatively been detected in Titan's atmosphere (Lai et al. 2017), which gives rise to the possibility that propyl cyanide might also be present. The most recent work of Stevenson et al. (2015) shows that these cyanides are the most favoured molecules to form thermodynamically stable membranes (azotosomes) in liquid methane at the surface temperature of Titan (90–95 K), and are therefore potential precursors for life. Our analysis yields precise spectroscopic parameters to also initiate a search for 3-methylbutyronitrile in Titan's atmosphere where nitrogen-bearing species appear to play a crucial role.

Another aspect of the detection and identification of molecules in space focusses on precursors of biologically relevant species in interstellar clouds. In this respect, many amino acids have already been identified on meteoritic material (Cronin & Pizzarello 1996; Cobb & Pudritz 2014; Martins et al. 2015). Most of these amino acids show a branched structure. The finding that meteoritic material shows such a rich and complex molecular inventory is proof that precursors of life have already been formed before the stage of planet and star formation. However, it is striking that *iso*-propyl cyanide is the only branched molecule that has been detected in interstellar environments up to now. If other branched molecules are present in the interstellar medium these will form the missing link between interstellar chemistry and the molecular composition of meteorites, comets, and planets.

We expect that our study will assist the detection and identification of other branched species in the interstellar and circumstellar medium. This study will help to shed light on the formation and destruction schemes of complex molecules in space.

Acknowledgements. We thank Oliver Zingsheim and Dennis Wachsmuth for help during the FTMW measurements in Hannover. We are grateful to Arnaud Belloche for communicating the results of a search for 3-methylbutyronitrile in the EMoCA survey. This work has been supported by the Deutsche Forschungsgemeinschaft (DFG) through the collaborative research grant SFB 956 "Conditions and Impact of Star Formation", project areas B4 and B3. Olivia Wilkins acknowledges support from a Fulbright U.S. Student Research Award.

References

Arenas, B. E., Gruet, S., Steber, A. L., Giuliano, B. M., & Schnell, M. 2017, Phys. Chem. Chem. Phys. (Incorporating Faraday Transactions), 19, 1751
Balle, T. J., & Flygare, W. H. 1981, Rev. Sci. Instrum., 52, 33
Becke, A. D. 1993, J. Chem. Phys., 98, 5648
Belloche, A., Garrod, R. T., Müller, H. S. P., & Menten, K. M. 2014, Science, 345, 1584
Belloche, A., Müller, H. S. P., Garrod, R. T., & Menten, K. M. 2016, A&A, 587, A91
Bocquet, R., Wlodarczak, G., Bauer, A., & Demaison, J. 1988, J. Mol. Spectr., 127, 382
Bohn, R. K., Pardus, J. L., August, J., Brupbacher, T., & Jäger, W. 1997, J. Mol. Struct., 413, 293
Brauer, C. S., Pearson, J. C., Drouin, B. J., & Yu, S. 2009, ApJS, 184, 133
Cazzoli, G., Cotti, G., Dore, L., & Kisiel, Z. 1993, J. Mol. Spectr., 162, 467
Cobb, A. K., & Pudritz, R. E. 2014, ApJ, 783, 140
Cordiner, M. A., Palmer, M. Y., Nixon, C. A., et al. 2015, ApJ, 800, L14
Cronin, J. R., & Pizzarello, S. 1996, Meteorit. Planet. Sci., 31
Crowder, G. A. 1988, Spectrosc. Lett., 21, 447
Crowder, G., & Carlisle, G. 1991, J. Comput. Chem., 12, 880
Daly, A. M., Bermúdez, C., López, A., et al. 2013, ApJ, 768, 81
Demyk, K., Mäder, H., Tercero, B., et al. 2007, A&A, 466, 255
Dunning, Jr. T. H. 1989, J. Chem. Phys., 90, 1007
Endres, C. P., Schlemmer, S., Schilke, P., Stutzki, J., & Müller, H. S. P. 2016, J. Mol. Spectr., 327, 95
Fortman, S. M., Medvedev, I. R., Neese, C. F., & De Lucia F. C. 2010a, ApJ, 714, 476
Fortman, S. M., Medvedev, I. R., Neese, C. F., & De Lucia F. C. 2010b, ApJ, 725, 1682
Frisch, M. J., Trucks, G. W., Schlegel, H. B., et al. 2016, Gaussian 09, Revision A.02 (Wallingford, CT: Gaussian, Inc.)
Garrod, R. T., Belloche, A., Müller, H. S. P., & Menten, K. M. 2017, A&A, 601, A48
Grabow, J.-U. & Stahl, W. 1990, Z. Naturforsch. A, 45, 1043
Grabow, J.-U., Palmer, E. S., McCarthy, M. C., & Thaddeus, P. 2005, Rev. Sci. Instrum., 76, 093106
Iglesias-Groth, S., Cataldo, F., Ursini, O., & Manchado, A. 2011, MNRAS, 410, 1447
Jahn, M. K., Dewald, D. A., Wachsmuth, D., Grabow, J.-U., & Mehrotra, S. C. 2012, J. Mol. Spectr., 280, 54
Johnson, D. R., Lovas, F. J., Gottlieb, C. A., et al. 1977, ApJ, 218, 370
Kisiel, Z. 1985, Chem. Phys. Lett., 118, 334
Kisiel, Z. 1989, J. Mol. Spectr., 135, 223
Kisiel, Z., Białkowska-Jaworska, E., Desyatnyk, O., Pietrewicz, B. A., & Pszczółkowski, L. 2001, J. Mol. Spectr., 208, 113
Kolesniková, L., Alonso, E. R., Mata, S., Cernicharo, J., & Alonso, J. L. 2017, ApJS, 233, 24
Lai, J. C.-Y., Cordiner, M. A., Nixon, C. A., et al. 2017, AJ, 154, 206
Lee, C., Yang, W., & Parr, R. G. 1988, Phys. Rev. B, 37, 785
Mäder, H., Heise, H. M., & Dreizler, H. 1974, Z. Naturforsch. A, 29, 164
Margulès, L., Motiyenko, R., Demyk, K., et al. 2009, A&A, 493, 565
Margulès, L., Belloche, A., Müller, H. S. P., et al. 2016, A&A, 590, A93
Martin-Drumel, M. A., van Wijngaarden, J., Zingsheim, O., et al. 2015, J. Mol. Spectr., 307, 33
Martins, Z., Modica, P., Zanda, B., & D'Hendecourt, L. L. S. 2015, Meteorit. Planet. Sci., 50, 926
Medvedev, I. R., & De Lucia F. C. 2007, ApJ, 656, 621
Mehringer, D. M., Pearson, J. C., Keene, J., & Phillips, T. G. 2004, ApJ, 608, 306
Møller, C., & Plesset, M. S. 1934, Phys. Rev., 46, 618
Müller, H. S. P., Thorwirth, S., Roth, D. A., & Winnewisser, G. 2001, A&A, 370, L49
Müller, H. S. P., Schlöder, F., Stutzki, J., & Winnewisser, G. 2005, J. Mol. Spectr., 742, 215
Müller, H. S. P., Coutens, A., Walters, A., Grabow, J.-U., & Schlemmer, S. 2011, J. Mol. Spectr., 267, 100
Müller, H. S. P., Brown, L. R., Drouin, B. J., et al. 2015, J. Mol. Spectr., 312, 22
Müller, H. S. P., Drouin, B. J., Pearson, J. C., et al. 2016a, A&A, 586, A17
Müller, H. S. P., Walters, A., Wehres, N., et al. 2016b, A&A, 595, A87
Müller, H. S. P., Zingsheim, O., Wehres, N., et al. 2017, J. Phys. Chem. A, 121, 7121
Nguyen, L., Walters, A., Margulès, L., et al. 2013, A&A, 553, A84
Ordu, M. H., Müller, H. S. P., Walters, A., et al. 2012, A&A, 541, A121
Palmer, M. Y., Cordiner, M. A., Nixon, C. A., et al. 2017, Sci. Adv., e1700022
Pearson, J. C., & Mueller, H. S. P. 1996, ApJ, 471, 1067
Pickett, H. M. 1991, J. Mol. Spectr., 148, 371
Pienkina, A. O., Margulès, L., Motiyenko, R. A., Müller, H. S. P., & Guillemin, J.-C. 2017, A&A, 601, A2
Remijan, A. J., Friedel, D. N., de Pater, I., et al. 2006, ApJ, 643, 567
Remijan, A. J., Milam, S. N., Womack, M., et al. 2008, ApJ, 689, 613
Richard, C., Margulès, L., Motiyenko, R. A., & Guillemin, J.-C. 2012, A&A, 543, A135
Solomon, P. M., Jefferts, K. B., Penzias, A. A., & Wilson, R. W. 1971, ApJ, 168, L107
Stevenson, J. M., Fouad, W. A., Shalloway, D., et al. 2015, Icarus, 256, 1
Tam, H. 1988, PhD Thesis, University of North Texas, USA
Tielens, A. G. G. M. 2013, Rev. Mod. Phys., 85, 1021